Spin-polarized fermions with *p*-wave interactions

Furkan Çağrı Top,* Yair Margalit,* and Wolfgang Ketterle
Research Laboratory of Electronics, MIT-Harvard Center for Ultracold Atoms, and Department of Physics, Massachusetts Institute of Technology, Cambridge, Massachusetts 02139, USA

(Received 14 September 2020; accepted 14 September 2021; published 15 October 2021)

We have created quantum degenerate Fermi gases of ^{6}Li atoms at unprecedented high densities exceeding $1/\lambda\!\!\!^{-3}$ (where λ is the wavelength of resonant light). In this regime, new optical properties are predicted. Spin-polarized Fermi gases are usually regarded as noninteracting due to the weakness of *p*-wave interactions. Here we study the properties of "*p*-wave matter," where elastic and inelastic *p*-wave collisions determine the dynamics of the system. We characterize thermalization, evaporative cooling, and inelastic two-body and three-body collisions. *P*-wave dipolar relaxation creates a metastable mixture of the lowest and highest hyperfine states.

DOI: 10.1103/PhysRevA.104.043311

I. INTRODUCTION

Single component Fermi systems are of fundamental interest. Even for weak interactions, they will show the Kohn-Luttinger instability [1] at very low temperatures and form Cooper pairs. Since *s*-wave interactions are not allowed in a single-component system, pairing and superfluidity can be unconventional. The A_1 superfluid phase of liquid helium-3 is an example of a single-component Cooper pair condensate [2], although the spin-polarization at high magnetic fields is at most in the percent range [3]. Triplet pairing may also occur in the superconductivity of strontium ruthenate [4]. For ultracold atomic gases, the de Broglie wavelength is much longer than the range of the van der Waals interactions, and therefore interactions in single component Fermi gases are very weak at low temperatures.

Here we explore to what extent we can enhance *p*-wave interactions by increasing the density of the gas until three-body recombination becomes too strong. We reach densities larger than 10^{15} cm^{-3} with lifetimes of more than a second. At these densities, the Fermi energy is 50 times larger than the single-photon recoil energy, and light scattering should be Pauli blocked [5–7]. At densities larger than $\lambda\!\!\!^{-3}$, the index of refraction should show strong dipolar corrections [8], resulting in shifts of the resonance larger than the natural linewidth [9].

In this paper, we focus on the characterization of *p*-wave collisions in this new high-density regime. An understanding of *p*-wave collisions is of general interest for ultracold atom science, molecular calculations and also for the most precise atomic clocks using strontium and ytterbium [10] in optical lattices where weak *p*-wave interactions cause shifts of the clock frequency [11]. Due to the weakness of *p*-wave interactions, the typical thermalization times of spin-polarized Fermi gases are on the order of tens of seconds, even at temperatures much higher than the degeneracy temperature [12]. Here we observe thermalization in ≈100 ms.

Our motivation has been to initiate a broader study to what extent high density can push single-component fermions into a new interesting system for few- and many-body physics without involving the usually lossy Feshbach resonances. For ^{6}Li, the atom studied here, a partial success was accomplished. The ratio of good to bad collisions was much better than near a recently studied Feshbach resonance [13]. This allowed to perform *p*-wave evaporative cooling which achieved modest efficiency, being limited by nonresonant three-body losses.

The scaling behavior of *p*-wave collisions is very different from *s*-wave collisions which dominate in most ultracold gas experiments. For *s*-wave collisions, the elastic cross section and the three-body recombination rate are constant near zero temperature, whereas for *p*-wave scattering, they both scale as T^2 or k^4 with the relative momentum $\hbar k$ of the colliding atoms. In the zero-range limit (i.e., when the effective range is negligible), the *p*-wave cross section σ_p is characterized by the *p*-wave scattering volume V_p as $\sigma_p(k) = 24\pi V_p^2 k^4$ [14]. For sufficiently small V_p, the three-body loss rate coefficient L_3 has the form $L_3 = C(\hbar/m)k^4 V_p^{8/3}$ with a dimensionless scaling constant C [15,16]. Evaporative cooling requires a favorable ratio of elastic to inelastic collision. For a Fermi gas with a temperature $T = T_F$, the elastic collision rate $\Gamma_{\rm el}$ is proportional to $V_p^2 k^8$ and three-body loss rate to $V_p^{8/3} k^{10}$, implying a ratio of good-to bad collisions which scales as $1/(CV_p^{2/3}k^2)$. This suggest that a favorable regime is at low density and weak *p*-wave interactions, i.e., far away from any *p*-wave Feshbach resonances. The existence of other loss mechanism (e.g., vacuum-limited trapping time) leads to a favorable regime at intermediate densities. Figure 1 shows that for the system studied here, ^{6}Li at low magnetic fields, there is a favorable window around $T_F = 150\ \mu$K, where the ratio of good to bad collisions peaks around 150, much better than achievable near a *p*-wave Feshbach resonance [13] (see Appendix A for a detailed comparison).

*These authors contributed equally to this work

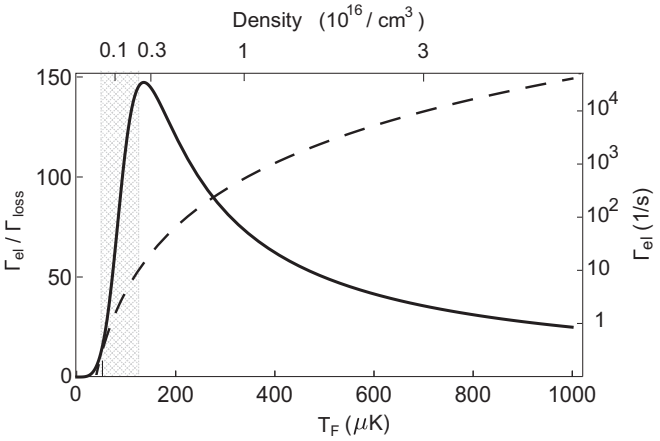

FIG. 1. The ratio of good (elastic) to bad (inelastic) collisions, and the elastic collision rate for ^{6}Li atoms near zero field, far away from the p-wave Feshbach resonance. The solid line shows the ratio for an harmonically trapped cloud with $T = T_F$ assuming a vacuum lifetime of 60 seconds. The dashed line is the elastic collision rate. In this work, we have explored the shaded region.

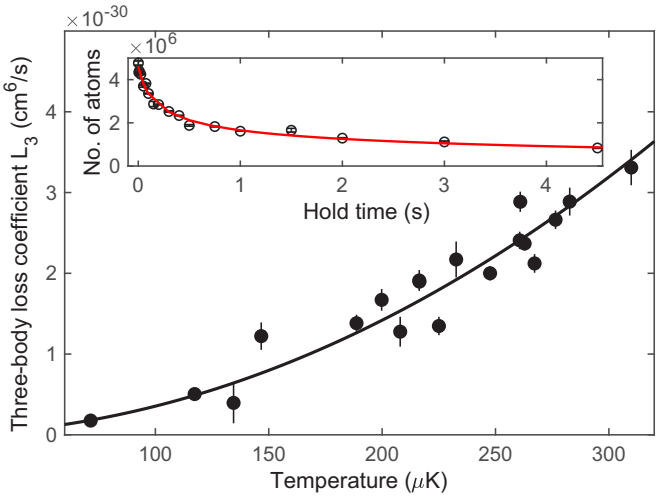

FIG. 2. Three-body loss for spin-polarized fermions. Different temperatures are realized by reducing the trap laser power. The three-body loss coefficient L_3 scales quadratically with temperature. The black line is a parabolic fit through the origin, resulting in $L_3 = (3.55 \pm 0.22) \times 10^{-23} \times T^2$. Error bars show the statistical one standard deviation uncertainties of the fit parameter L_3 used to describe the atom number decay. The inset shows the decay curve at $T = 310$ μK and its fit to Eq. (1).

We note that the k^4 scaling makes p-wave evaporation different from evaporative cooling with single component dipolar gases (as observed in Ref. [17]), where higher partial waves are not suppressed at low temperatures, and the elastic cross section is constant even at $T = 0$, whereas the p-wave cross section freezes out proportional to T^2.

II. SAMPLE PREPARATION

The ultracold lithium clouds are prepared in the following way. After laser cooling of ^{23}Na and ^{6}Li in a double species MOT and optical pumping of the Li (Na) atoms to the stretched state $|F = 3/2, m_F = +3/2\rangle$ ($|2, +2\rangle$), the atoms are captured in a plugged quadrupole magnetic trap [18] and sympathetically cooled through forced microwave evaporation of the Na atoms [19]. During the last part of the evaporation, a single-beam 1064-nm optical dipole trap (ODT) with a variable spot size is turned on. The spot size is controlled by a variable-aperture iris shutter, which is initially set to a small open diameter, producing an optical trap with large volume and shallow depth. This keeps the densities low ($\sim 10^{12}$ cm^{-3}) and avoids inelastic collisions. Finally, the quadrupole field is turned off, and the remaining Na atoms are expelled using a pulse of resonant light. The Li atoms are then transferred to the collisionally stable lowest Zeeman state $|1/2, 1/2\rangle \equiv |1\rangle$ using an RF Landau-Zener sweep. Subsequently, the iris is opened to its full aperture in 0.5 sec, thus reducing the $(1/e^2)$ ODT spot size radius from approximately 29 to 8 μm and compressing the cloud to densities up to 10^{15} cm^{-3}. In order to reduce three-body losses during the iris opening, the 1064 nm laser power is reduced to 30% of its maximum power. The variable spot size ODT is critical to bridge three orders magnitude in density between initial evaporative cooling and the experiment.

Finally, the ODT power is ramped up to the maximum power of 6.2 W. The cloud is held in this tight and deep trap for 30 ms to ensure thermal equilibrium. A characteristic sample contains $\sim 5.3 \times 10^6$ Li atoms at 300 μK temperature and $T/T_F = 0.75$, where T_F is the Fermi temperature. The corresponding density is $n = 1.3 \times 10^{15}$ cm^{-3}. The trapping frequencies are $(\omega_{rx}, \omega_{ry}, \omega_z) = (91.5, 102, 2)$ kHz, which are measured by exciting dipole or breathing oscillations. Since p-wave interactions are weak, the possibility of impurity populations of ^{6}Li in other hyperfine states or of Na is a possible concern because they can undergo much faster s-wave collisions. However, these impurities should be rapidly purged from the sample via fast s-wave inelastic collisions. With absorption imaging, we set an upper bound of 0.01% for Na or for Li in the upper hyperfine state $|F = 3/2\rangle$ and in state $|1/2, -1/2\rangle \equiv |2\rangle$.

III. THREE-BODY LOSS MEASUREMENTS

For ^{6}Li atoms in the lowest hyperfine state, there are no inelastic two-body collisions. Three-body collisions for fermions are suppressed by k^4 for three identical fermions and by k^2 for fermions in two states [20]. So far, ^{6}Li three-body recombination has been studied only near a Feshbach resonance which can enhance three-body loss coefficient by six orders of magnitude [16], and in a spin mixture with s-wave interactions [21]. Due to the high densities achieved here, we are sensitive to background p-wave losses (i.e., at a field of 1 G, far away from the 1-1 Feshbach resonance located at 159 G).

We observe three-body decay by monitoring the decrease in the number of trapped atoms (Fig. 2). The rate of change of the number of trapped atoms N is given by

$$\dot{N} = L_1 N - L_3 \langle n^2 \rangle N, \tag{1}$$

where the density independent losses, parametrized by L_1 are almost negligible with $1/L_1 = 31.1 \pm 1.3$ sec. The

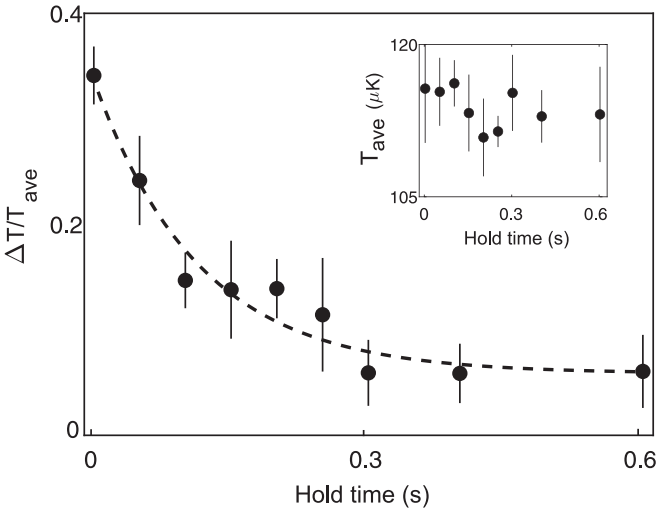

FIG. 3. Observation of cross-dimensional thermalization. Normalized temperature difference $\Delta T/T_{\rm ave}$ between the radial and axial directions as a function of hold time after creating a sample with anisotropic energy distribution. The dashed line is an exponential fit $\Delta T/T_{\rm ave} = A\exp(-\Gamma_{\rm th}t) + c$. The temperature difference has a small (5%) offset in all measurements the reason for which we have not tracked down (possibly due to anisotropic heating/cooling or nonsudden switch-off of potentials to initiate ballistic expansion). Inset shows the average temperature, demonstrating that there is no heating during the measurement. Error bars represent the standard deviation of the data averaged over three measurements.

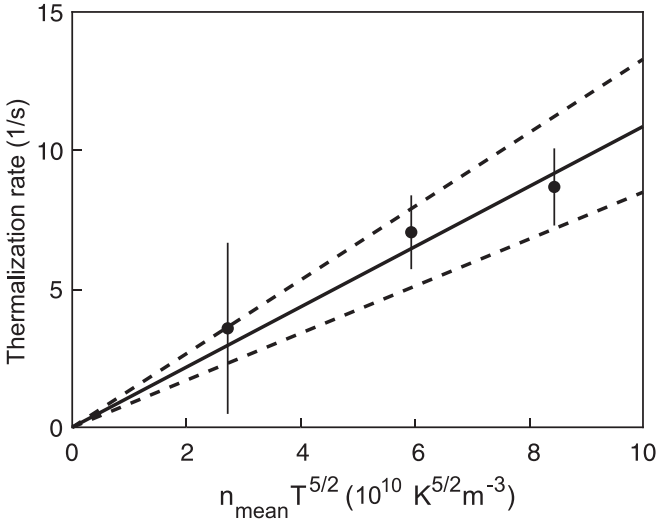

FIG. 4. Determination of the background p-wave scattering length. Thermalization rates $\Gamma_{\rm th}$ were measured for a range of atom numbers and temperatures and are shown as a function of the mean density times $T^{5/2}$, which is the scaling with density and temperature given by Eq. (2). A linear fit weighing the data with inverse of variances (vertical error bars) gives the p-wave background scattering length $|V_p| = (39^{+1.3}_{-1.6}\, a_0)^3$. The dashed lines represent the 95% confidence interval of the fit. We note that the only fit parameter is the slope, representing V_p.

actual analysis accounts for changes in temperature and cloud size as a function of hold time, and the anharmonic trapping potential (see Appendix B). The results in Fig. 2 confirm the quadratic scaling of L_3 with temperature according to a Wigner threshold law [20], as already observed near a p-wave Feshbach resonance [16]. At 100 μK temperature, we obtain $L_3 = (3.55 \pm 0.22) \times 10^{-31}$ cm^6/sec, which is among the smallest three-body rate coefficients observed for ultracold atoms, illustrating the high stability of spin-polarized Fermi gases. Thermal gases of sodium and rubidium, for example, have rate coefficients between 10^{-29} and 10^{-28} cm^6/sec [22–24].

Using the data in Fig. 2, we obtain a dimensionless scaling constant value of $C = (3.0 \pm 0.6) \times 10^4$, compared to the value of $C = 2 \times 10^6$ reported in Ref. [16] near the Feshbach resonance. While bosons show a universal character of three-body losses (i.e., the loss coefficient is independent of the details of the interatomic potential [25]), the different C coefficient values demonstrate for the first time the lack of universal character in recombination of three ultracold fermions, as has been hypothesized in Ref. [15].

IV. THERMALIZATION MEASUREMENTS

Elastic collision rates are observed by creating a nonequilibrium state and monitoring the collisional relaxation back to equilibrium [12,26]. In order to avoid systematic errors due to three-body losses, heating, and trap anharmonicities, the atom number is lowered to three different values around 10% of its maximum value. An anisotropic temperature (with up to 35% temperature difference between the radial and axial directions) is created by spilling atoms out of the trap in the axial direction by decreasing the trap laser power, and adding a magnetic field gradient along the axial direction. We note that the more common parametric excitation technique has limited effectiveness for our cloud (possibly due to Pauli blocking of the parametric heating process). The magnetic gradient is then turned off and the ODT power is nonadiabatically ramped back up to the full power. Thermal relaxation by p-wave collisions is observed by monitoring the time evolution of the temperature difference between axial and radial directions.

A typical thermalization measurement is shown in Fig. 3. The thermalization rate $\Gamma_{\rm th}$ is obtained from an exponential fit to the decay curve of the temperature difference. The thermalization rate is proportional to the elastic collision rate ($\Gamma_{\rm th} = \Gamma_{\rm el}/\alpha$), where α is the average number of elastic collisions necessary for the cross-dimensional thermalization. An analytical calculation of the energy exchange in a Boltzmann gas gives $\alpha = 64/15$ for p-wave collisions [27] which agrees with a value $\alpha = 4.1$ obtained from Monte Carlo simulations [12]. Using the thermally averaged p-wave elastic collision rate, we obtain an expression for the thermalization rate (see Appendix C)

$$\Gamma_{\rm th} = \frac{1152}{\alpha}\sqrt{2\pi}\frac{V_p^2\mu^{3/2}}{\hbar^4} n_{\rm mean}(k_B T)^{5/2}, \qquad (2)$$

where μ is the reduced mass of two ^{6}Li atoms, and $n_{\rm mean}$ the average atomic density.

Figure 4 shows the measured thermalization rates as a function of $n_{\rm mean}T^{5/2}$. A linear fit determines the background p-wave scattering volume of state $|1\rangle$ to be $|V_p| =$

$(39^{+1.3}_{-1.6}\, a_0)^3$, where a_0 is the Bohr radius. This value is in reasonable agreement with theoretically calculated values of $(-35.3a_0)^3$ [28] and $(-36a_0)^3$ [29], and is the first experimental measurement of a background scattering volume [30]. This measurement was done at a magnetic field of 1 G, far away from the 1-1 Feshbach resonance located at 159 G. However, there may still be a small contribution from the wings of the resonance which decreases the scattering volume at low fields by $\Delta B/(B - B_{\rm res})$ or 25%, assuming a resonance width of $\Delta B = 40$ G [31]. This corrects the background scattering volume to $(42a_0)^3$.

V. EVAPORATIVE COOLING

As shown in Fig. 1, for a range of temperatures and densities, the measured elastic collision rates are much higher than the inelastic loss rates, allowing for evaporative cooling, using the following procedure. After sample preparation, the optical trap is ramped down to a fifth of its original power, where the ratio of good to bad collisions is around 70, and the ratio of the trap depth to temperature is $\eta = 7$. The trap depth is then reduced by a magnetic force applied in the axial direction which is ramped up to various values during 1.5 second. This "tilt evaporation" maintains the confinement and is superior compared to simply reducing the laser beam power [32]. A square root time dependence of the ramp is used to follow the decreasing elastic collision rate. After turn-off of the magnetic field gradient, the optical trap is restored to its full value, and a time-of-flight absorption image measures the velocity distribution [Fig. 5(a)]. By performing the analysis always with atoms released from the original trap, we avoid systematic effects in comparing different trapping potentials, e.g., anharmonicities.

We monitor the results of evaporation by determining the final temperature from a Gaussian fit to the wings of the time-of-flight distribution, and the Fermi temperature from the measured number of atoms N and trap frequencies (according to $k_B T_F = \hbar(\omega_{rx}\omega_{ry}\omega_z 6N)^{1/3}$ [33]). Figure 5(b) shows a decrease in temperature and T/T_F as the final trap depth is lowered (by increasing the magnetic force). The calculated ratio of good to bad collisions decreases from 70 to 23. The increase in degeneracy is rather modest, since a ratio of good to bad collisions of around 50 will allow evaporative cooling only with modest efficiency. For this ratio, the γ parameter (increase in the logarithm of the phase space density over logarithm of atom loss) is at best around 1 [34], where the experimental value is $\gamma = 0.94$.

The clouds after evaporation are not fully equilibrated: The Fermi-Dirac profile calculated with the fitted values for T and T_F do not match well with the observed profiles [Fig. 5(c)]. The deeper the evaporation progresses, the larger is the disagreement. We ascribe the lower population for low velocities to the strong velocity dependence of p-wave collisions (see Appendix D). Equilibrium in the cloud is quickly established when we use a diabaic Landau-Zener sweep to admix 10% spin impurities (atoms in state $|2\rangle$) right after the evaporation ramp which undergo s-wave collisions with the atoms in state $|1\rangle$ [Fig. 5(d)].

We have observed nonequilibrium distributions also after cross-sectional thermalization (as measured in Fig. 3) showing that full thermalization takes longer than the so-called thermalization time for distributing energy isotropically, an effect which has not been pointed out before and is discussed in Appendix D. Therefore p-wave collisions are less efficient for evaporative cooling than s-wave collisions, and require a considerable higher ratio of good to bad collisions.

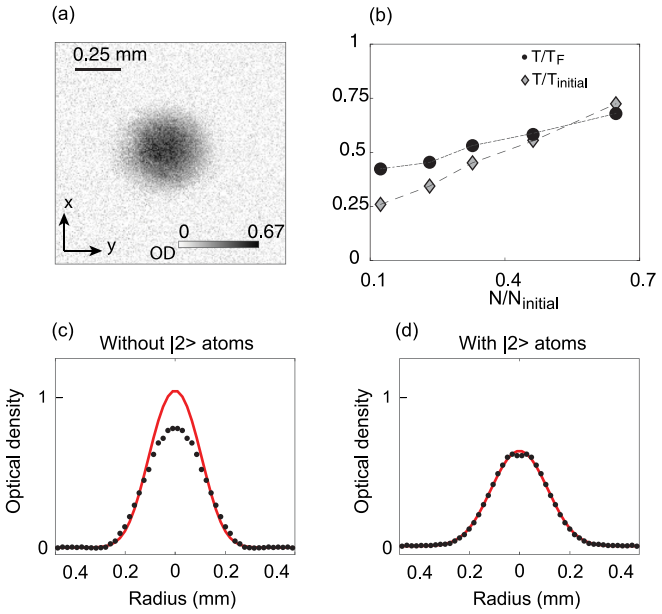

FIG. 5. Evaporative cooling using p-wave collisions. (a) Time-of-flight absorption image (average of 4 shots) of degenerate atoms at $T/T_F = 0.42$. Temperature is determined from a Gaussian fit to the wings of the cloud, and Fermi energy is calculated using measured number of atoms and trapping frequencies [33]. (b) Evolution of T/T_F for different final trap depths and therefore different final numbers of atoms. [(c) and (d)] Comparison of the azimuthally averaged radial cloud profiles, before (c) and after (d) introducing a second spin component of state $|1/2, -1/2\rangle \equiv |2\rangle$ which undergoes s-wave collisions with state $|1\rangle$. Red lines show the Fermi-Dirac profile set by the atom number, temperature and trapping frequencies. The cloud in (c) is not in thermal equilibrium, in contrast to (d). Note that the number of atoms in (d) is lower, probably due to enhanced three-body loss.

VI. DIPOLAR RELAXATION OF STATE $|6\rangle$

In the magnetic trap, we cool lithium atoms in state $|3/2, 3/2\rangle \equiv |6\rangle$. By omitting the Landau-Zener sweep in the sample preparation, we can study collisional properties of state $|6\rangle$ clouds. Initial measurements of thermalization rates found the surprising result that thermalization in state $|6\rangle$ is much faster than in state $|1\rangle$. It turned out that this is due to an admixture of state $|1\rangle$ atoms in a quasi-equilibrium concentration. This is caused by a rather amazing interplay of various collision processes: p-wave dipolar relaxation of state $|6\rangle$ atoms, ultrafast (μs) s-wave spin relaxation between state $|6\rangle$ and state $|3/2, 1/2\rangle \equiv |5\rangle$ atoms in which state $|5\rangle$ decays to state $|1\rangle$, fast collisional relaxation by s-wave elastic collisions between states $|1\rangle$ and $|6\rangle$ and loss of state $|1\rangle$ atoms by three-body recombination.

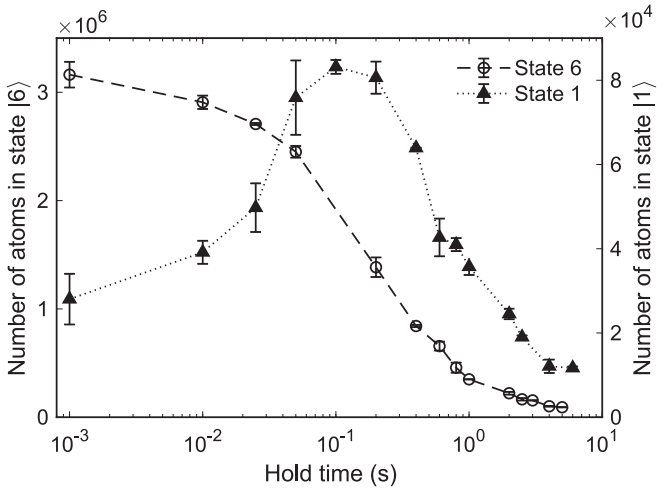

FIG. 6. Dipolar relaxation of state $|6\rangle$, leading to a population of state $|1\rangle$. Population of both states, as a function of hold time in the trap at full power. Lines are a guide to the eye. The initial number of state $|1\rangle$ atoms are generated while the optical trap was ramped up to full power.

Via absorption imaging, we find that a pure state $|6\rangle$ cloud creates a growing admixture of state $|1\rangle$ atoms (Fig. 6). Although our detection scheme is sensitive to both states $|1\rangle$ and $|2\rangle$ of the lower $F = 1/2$ hyperfine level, we can exclude the presence of state $|2\rangle$ since it undergoes rapid spin relaxation with state $|6\rangle$ (with a rate coefficient of 10^{-8} cm^3/s at 1 G field [35]).

The dominant decay mechanism for state $|6\rangle$ atoms is three-body loss. From the initial slope of the decay, we obtain a loss rate of $\dot{N}/N = -6.3$/s, slightly larger than observed for state $|1\rangle$ under the same conditions. A second, weaker loss mechanism is p-wave dipolar relaxation which transfers spin angular momentum to orbital angular momentum [36]. The rate coefficient for producing state $|5\rangle$ atoms is calculated to be $L_2^{\rm dip} = 3.2 \times 10^{-16}$ cm^3/s [36]. A generated state $|5\rangle$ atom undergoes rapid spin relaxation with state $|6\rangle$ atoms to state $|1\rangle$ with a predicted rate coefficient of 2×10^{-9} cm^3/s [37]. At our densities, this spin flip takes place in less than 1 μs, one of the fastest collisional processes ever observed with ultracold atoms. This spin flip releases the ground state hyperfine splitting energy of 11 mK (three times the trap depth). Our detection of cold and trapped state $|1\rangle$ atoms implies that the cloud is collisionally dense for collisions between states $|1\rangle$ and $|6\rangle$. A collisional density of one along the radial direction requires an s-wave scattering length of around $200a_0$. We don't know of any predictions for 6-1 scattering length, but the 6-2 scattering length is predicted to be large (around $-1700a_0$ [35]) due to the large triplet scattering length for ^{6}Li of $-2160a_0$ [37]. Note that all states should decay rapidly in spin relaxation collisions with state $|6\rangle$, except for state $|1\rangle$, for which spin relaxation is not possible due to conservation of angular momentum along the z direction.

The observed initial growth rate in the number of state $|1\rangle$ atoms of $\dot{N}_1 = 1.06 \times 10^6$ atoms/s is in reasonable agreement with the predicted production of state $|5\rangle$ atoms by dipolar relaxation, and implies a capture efficiency close to unity. After 1 s, the relative population in state $|1\rangle$ reaches a quasi-equilibrium, indicating a loss mechanism for state $|1\rangle$ with a rate of around 10/s. State $|1\rangle$ can disappear in three-body recombination with possible combinations of states 6,6,1 or 6,1,1 or 1,1,1. Since some of the rate coefficients are not known, we cannot model the dynamics. The observation of a quasi-constant fraction of state $|1\rangle$ atoms suggests that the ratio of production and loss rate is proportional to the density of state $|6\rangle$ atoms.

VII. DISCUSSION

In this paper, we have explored a spin-polarized Fermi gas at unprecedentedly high densities and observed various collisional interactions. Although the observed elastic collision cross section of 9×10^{-16} cm^2 is four orders of magnitude smaller than typical s-wave cross sections of 7×10^{-12} cm^2, these Fermi gases equilibrate on time scales of 100 ms and establish a weakly interacting gas for which the p-wave mean field energy is 0.2% of the Fermi energy (for zero temperature and 10^{15} cm^{-3} density [38]). This study has realized extreme parameters for ultracold atoms, not only in density, but also in Fermi energies (3 MHz) and in inelastic collision times (<1 μs), and found new effects in p-wave thermalization. Further improvements, also in p-wave evaporative cooling, can be achieved in optimized traps, with improved vacuum lifetime, and by exploring other atoms, states or magnetic field ranges. In the near future, we plan to use these unprecedented high densities and optical densities for studies of superradiance and light scattering in new regimes.

ACKNOWLEDGMENTS

We thank Hyungmok Son for comments on the manuscript. We acknowledge support from the NSF through the Center for Ultracold Atoms and Grant No. 1506369, ARO-MURI Non-Equilibrium Many-Body Dynamics (Grant No. W911NF-14-1-0003), AFOSR- MURI Quantum Phases of Matter (Grant No. FA9550-14-10035), ONR (Grant No. N00014-17-1-2253), and from a Vannevar-Bush Faculty Fellowship.

APPENDIX A: RATIO OF GOOD TO BAD COLLISIONS

Here we provide a more detailed discussion of the role of elastic and inelastic collisions. An obvious question is whether Feshbach resonances can lead to a more favorable ratio of elastic to inelastic collisions. Comprehensive studies of the p-wave resonance near 159 G have been carried out by the Tokyo group [13,16]. In the regime with universal scaling (Eq. (4) in Ref. [16]), the losses are 67 times higher than for the background interactions studied here. However, effective range corrections can enhance elastic collisions on one side of the resonance and suppress them on the other side; they also increase losses. As we discuss below, an analysis of the results of Refs. [13,16] show a narrow range of magnetic field detunings where the ratio of good-to-bad collisions is around 10, but at rather slow elastic collision rate around 5/s.

For the condition of our experiment, the zero-range approximation is valid, and the ratio of good to bad collisions

for the experimentally determined collision parameters (L_3, V_p) is shown in Fig. 1 of the main text. In the main text, we showed that the ratio of good to bad collisions scales as $1/(CV_p^{2/3}k^2)$. If we rewrite the scaling as $(T_F/\Gamma_{\rm el})^{1/3}/C$, and assume that a certain elastic collision rate is needed to overcome residual gas collisions, then the collision ratio depends only on the achievable densities (or T_F) and the constant C. We have measured the constant C for background scattering to be almost two orders of magnitude less than observed near a Feshbach resonance (see Sec. III). Therefore, in the regime where the zero-range approximation applies, the p-wave Feshbach resonance near 159 G has an unfavorable ratio of good to bad collisions.

However, near the Feshbach resonance, the zero-range approximation breaks down. For elastic collisions, the effective range term interferes constructively with the p-wave scattering volume on the high-field side of the resonance (and destructively on the other side), which can improve the collision ratio, as we show here.

The thermally averaged elastic collision rate is given by

$$\Gamma_{\rm el} = n_{\rm mean}\,\langle \sigma_{pFR}(k) v_{\rm rel}\rangle\,, \tag{A1}$$

where $v_{\rm rel}$ is the relative velocity between colliding atoms, and $n_{\rm mean} = \langle n\rangle = \frac{1}{N}\int n^2(\mathbf{r})d^3r$ is the mean density (sometimes referred to as the density-weighted density), given by $n_{\rm mean} = \frac{1}{48}(\frac{k_B m}{\hbar^2\pi})^{3/2}\frac{T_F^3}{T^{3/2}}$ for an harmonically trapped Boltzman gas. The p-wave cross section $\sigma_{pFR}(k) = 24\pi|f_{pFR}(k)|^2$ is expressed by the scattering amplitude $f_{pFR}(k)$. Near a p-wave Feshbach resonance, one can express the scattering amplitude using the effective range expansion [28] as

$$f_{pFR}(k) = \frac{k^2}{-\frac{1}{V(B)} + k_e k^2 - ik^3}, \tag{A2}$$

where k_e is the second coefficient in the effective-range expansion, and the scattering volume varies as $V(B) = V_p(1 + \frac{\Delta B}{B-B_{res}})$. We use the values from Ref. [13] to parametrize the Feshbach resonance: $V_p = (-41a_0)^3$, $k_e = -0.058a_0^{-1}$ and $\Delta B = 40G$.

Inelastic collisions near the p-wave Feschbach resonance have been parametrized through the scaling relation

$$\Gamma_{\rm inel} = \langle n^2\rangle L_3 = \langle n^2\rangle C\frac{\hbar}{m}k_T^4 V_B^{8/3}, \tag{A3}$$

where $\langle n^2\rangle = \frac{1}{N}\int n^3(\mathbf{r})d\mathbf{r}$ is the mean squared density, given by $\langle n^2\rangle = \frac{1}{864\sqrt{3}}(\frac{k_B m}{\hbar^2\pi})^3\frac{T_F^6}{T^3}$ for a harmonically trapped Boltzman gas, $k_T = \sqrt{3mk_BT/2\hbar^2}$, $C = C_0\{1 + (\beta k_e k_T^2 V_B)^\gamma\}$, $C_0 = 2\times 10^6$, $\beta = 9$, and $\gamma = 14$ [16].

With a vacuum limited lifetime of $\tau_{\rm vac} = 60$ seconds, we define ratio of good to bad collisions as

$$\frac{\Gamma_{\rm el}}{\Gamma_{\rm inel} + 1/\tau_{\rm vac}}. \tag{A4}$$

Figure 7(a) shows the ratio of good to bad collisions around the Feshbach resonance in the range relevant to the Tokyo group experiment [13]. The maximum of the ratio is around 12. Figure 7(b) shows the elastic collision rate.

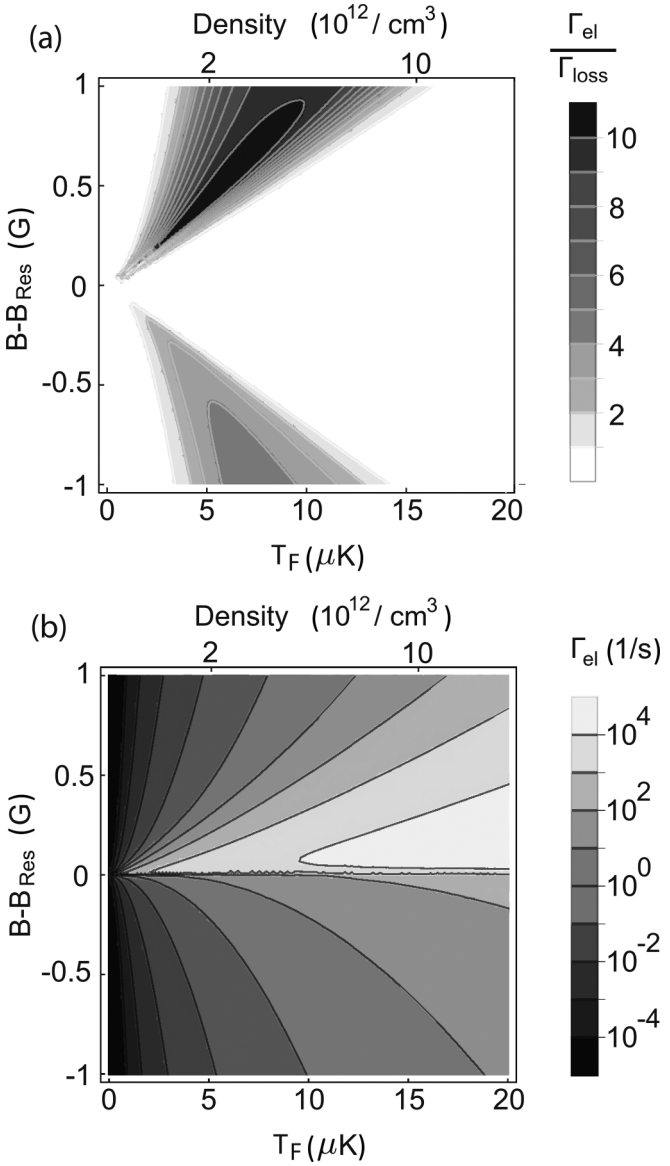

FIG. 7. The ratio of good to bad collisions (a) and the elastic collision rate (b) near the p-wave Feshbach resonance at 159 G for a harmonically trapped cloud with $T = T_F$.

APPENDIX B: ANALYSIS OF THREE-BODY LOSS DATA

1. Harmonic approximation

Since there are no inelastic two body collisions for ^{6}Li atoms in the lowest hyperfine state (i.e. the two-body loss coefficient $L_2 = 0$), the time dependence of the number of atoms N in the trap is described by the differential equation $\frac{\dot N}{N} = -L_3\langle n^2\rangle$. Later, we will add a single-particle loss rate L_1. For a nondegenerate cloud, and using the harmonic approximation for the trapping potential, the density profile is Gaussian, and we obtain

$$\frac{\dot N}{N} = -L_3\frac{N^2}{24\sqrt{3}\pi^3\sigma_x^2\sigma_y^2\sigma_z^2} = -L_3\frac{N^2}{24\sqrt{3}\pi^3 V^2}, \tag{B1}$$

where $\sigma_i = \sqrt{k_B T/m\omega_i^2}$ is the cloud's size in direction i, and the volume is defined as $V^2 = \sigma_x^2\sigma_y^2\sigma_z^2$. The Wigner threshold law predicts that L_3 should scale with wavenumber k as $L_3 \sim k^4$ [20]. Since three-body losses also cause significant heating during the measurement, L_3 and the volume V are both time-dependent, which has to be included in the analysis. Integrating both sides of the differential equation, we obtain

$$\frac{\dot{N}}{N^3} = -\frac{1}{24\sqrt{3}\pi^3}\frac{L_3(t)}{V^2(t)},$$
$$\frac{1}{2N^2} = \frac{1}{24\sqrt{3}\pi^3}\int_0^t \frac{L_3(t')}{V^2(t')}dt' + \frac{1}{2N_0^2}. \tag{B2}$$

We define $\Gamma_{3b}(t) = \frac{L_3(t)}{V^2(t)}$. Further simplifying the equation

$$\frac{1}{2N^2} = \frac{1}{24\sqrt{3}\pi^3}\Gamma_{3b}(0)\int_0^t \frac{\Gamma_{3b}(t')}{\Gamma_{3b}(0)}dt' + \frac{1}{2N_0^2},$$
$$N(\tilde{t}) = \sqrt{\frac{1}{\frac{1}{12\sqrt{3}\pi^3}\Gamma_{3b}(0)\tilde{t} + \frac{1}{N_0^2}}}, \tag{B3}$$

where

$$\tilde{t} = \int_0^t \frac{\Gamma_{3b}(t')}{\Gamma_{3b}(0)}dt' = \int_0^t \frac{T(0)}{T(t')}dt' \tag{B4}$$

is the rescaled time, $T(t)$ the time-dependent temperature, and we have used $\Gamma_{3b} \sim 1/T$. Knowledge of the temperature evolution from the experimental measurements allows us to calculate $\tilde{t}$, which can be used in the new time axis in the fit.

2. Beyond the harmonic approximation

The optical trapping potential is approximately Gaussian in the radial direction, and Lorentzian axially. If the ratio of the trap depth to the temperature $\eta \equiv U_0/k_B T$ is smaller than ~10, anharmonic corrections become important, and the expression in Eq. (B1) overestimates the density. One then has to numerically calculate the mean squared density $\langle n^2\rangle$, as we discuss below.

For temperatures $k_B T \gg \hbar\omega$, we can use a semiclassical description where the occupation of a phase space cell $\{\mathbf{r}, \mathbf{p}\}$ is given by a Boltzmann distribution: $f(\mathbf{r}, \mathbf{p}) \propto \exp[-\beta(\mathbf{p}^2/2m + U(\mathbf{r}))]$, where $U(\mathbf{r})$ is the external potential. The density distribution of the thermal gas is then given by integrating over the momentum:

$$n_{\rm th}(\mathbf{r}) = \frac{1}{C}\int \frac{d^3\mathbf{p}}{(2\pi\hbar)^3} f(\mathbf{r}, \mathbf{p})$$
$$= \frac{1}{C}\frac{(mk_B T)^{3/2}}{2\sqrt{2}\pi^{3/2}\hbar^3}\exp[-\beta U(\mathbf{r})]. \tag{B5}$$

The normalization constant C is determined by the total number of atoms N:

$$C = \frac{1}{N}\int \frac{(mk_B T)^{3/2}}{2\sqrt{2}\pi^{3/2}\hbar^3}\exp[-\beta U(\mathbf{r})]d^3\mathbf{r}. \tag{B6}$$

The mean squared density $\langle n^2\rangle$ is then given by

$$\langle n^2\rangle = \frac{1}{N}\int n_{\rm th}(\mathbf{r})^3 d^3 r$$
$$= \frac{N^2}{(2\pi)^2}\frac{\iint r\exp[-3\beta U(\mathbf{r})]drdz}{\left(\iint r\exp[-\beta U(\mathbf{r})]drdz\right)^3}, \tag{B7}$$

where $rdrdz$ is the volume element in cylindrical coordinates.

Without the harmonic approximation of $U(\mathbf{r})$ this integral is generally not analytically solvable. We evaluate it numerically, using the explicit potential of a focused Gaussian beam [33]:

$$U_{\rm ODT}(\mathbf{r}) = -\frac{U_0}{1 + (z/z_R)^2}\exp\left(-\frac{2r^2}{w(z)^2}\right), \tag{B8}$$

where $w(z) = w_0\sqrt{1 + (z/z_R)^2}$ is the beam spot size, z_R is the Rayleigh range of the beam, and U_0 is the trap depth.

Since gravity tilts the potential, it sets a constraint on the maximum energy an atom can have inside the trap. We include this effect by setting the integration limits to 95% of the full trap depth, i.e., $U_{\rm ODT}(r_{\rm max}) = 0.95U_0$, and $U_{\rm ODT}(z_{\rm max}) = 0.95U_0$. Without this cutoff, $\langle n^2\rangle$ tends towards zero.

To account for the scaling of the three-body loss coefficient with temperature, we modify Eq. (B1) such that $\dot{N} = L_1 N - L_3^T T^2\langle n^2\rangle N$, where L_3^T is the temperature-independent part of L_3. We insert the numerically calculated time-dependent $\langle n^2\rangle$ into the modified form of Eq. (1), and fit the decay of the atom number as a function of hold time. The values shown in Fig. 2 represent the loss coefficient at the beginning of each measurement (i.e., at zero hold time).

APPENDIX C: CALCULATION OF THE p-WAVE SCATTERING RATE

The thermally averaged p-wave elastic collision rate is given by

$$\Gamma_{\rm el} = n_{\rm mean}\langle\sigma_p(k)v_{\rm rel}\rangle$$
$$= n_{\rm mean}\sqrt{\frac{8}{\mu\pi}}(k_B T)^{-3/2}24\pi\int |f_p(k)|^2 E e^{-\beta E}dE. \tag{C1}$$

Far-away from the Feshbach resonance, and in the low energy limit, the scattering p-wave scattering amplitude [Eq. (A2)] becomes $f_{pFR}(k) \approx -V_p k^2$. This assumes that contributions from an effective range expansion are negligible, which should be well fulfilled in the low k limit [29], specifically when $k|V_p^{1/3}| \ll 1$ [39], which is valid in our case. The p-wave scattering cross-section for identical fermions is then given by

$$\sigma_p(k) = 24\pi|f_p(k)|^2 = 24\pi V_p^2 k^4, \tag{C2}$$

where V_p is the p-wave background scattering volume. The integral over the energy then gives $V_p^2\frac{4\mu^2}{\hbar^4}\frac{24}{\beta^5}$, where we used $E = \hbar^2k^2/2\mu$ for the collision energy, and where μ is the reduced mass. Combining all terms, and using $\Gamma_{\rm th} = \Gamma_{\rm el}/\alpha$, one directly obtains Eq. (1) of the main text.

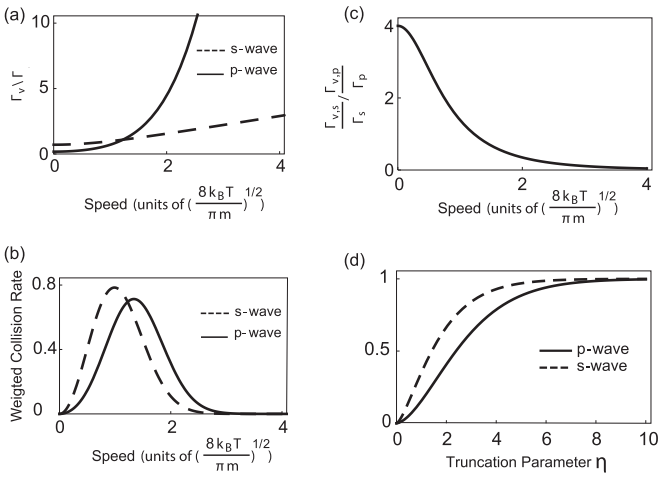

FIG. 8. Comparison between s- and p-wave collision rates. (a) shows the rate of collisions involving an atom with speed v with respect to the thermally averaged collision rate. In (b), the collision rates are weighted by the Maxwell-Boltzman speed distribution. (c) shows the ratio of s- and p-wave collisions for an atom at speed v. (d) is the fraction of collisions up to a kinetic energy of $\eta k_B T$, where η is the truncation parameter.

APPENDIX D: COMPARING *s* AND *p*-WAVE COLLISION RATES

Here we analyze how the k^4 dependence of the p-wave scattering cross-section affects thermal equilibration, and compare to the familiar case of s-wave scattering. The collision rate for partial wave l involving an atom with speed v is

$$\Gamma_{l,v} = n_{\text{mean}} \int \sigma_l |\mathbf{v} - \mathbf{v_2}| f_{v2} d^3 v_2, \tag{D1}$$

where σ_l is the collision cross-section, and f_v is the Maxwell-Boltzmann velocity distribution. We are interested in the ratio of the elastic scattering rate for an atom with velocity v compared to the average scattering rate:

$$\frac{\Gamma_{p,|\mathbf{v_1}|=v}}{\Gamma_p} = \frac{\sqrt{2}}{48} \int_0^\infty \int_0^\pi (\tilde{u}^2 + u^2 - 2\tilde{u}u\cos\theta)^{5/2} \times \sin\theta d\theta e^{-u^2} u^2 du \tag{D2}$$

and

$$\frac{\Gamma_{s,|\mathbf{v_1}|=v}}{\Gamma_s} = \frac{1}{\sqrt{2}} \int_0^\infty \int_0^\pi \sqrt{\tilde{u}^2 + u^2 - 2\tilde{u}u\cos\theta} \times \sin\theta d\theta e^{-u^2} u^2 du, \tag{D3}$$

where $\beta \frac{m}{2} v^2 = \tilde{u}^2$. Figure 8 shows these collision rates and their ratio. Considering the mean speed is $\sqrt{\frac{8k_BT}{\pi m}}$, s-wave interactions have three times more collisions for speeds below the average speed [Fig. 8(b)]. Detailed balance implies that the rate of collisions generating low-speed particles is the same as the rate of collisions involving a low-speed particle. In evaporative cooling the high-energy tail of the atomic distribution is removed, and collisions repopulate the tail and transfer population to lower velocities. For the same average collision rate, the transfer of population to the velocity group near $v = 0$ takes 4 times longer for p wave collisions compared to s wave [panel (c)]. In addition, for a trap depth of $\eta k_B T$ with $\eta = 5$, the rate of p-wave collisions calculated for a full Boltzmann distribution overestimates the collision rate of the truncated Boltzmann distribution by 13% [panel (d)]. As a result, efficient evaporation with p-wave collisions requires a substantially higher ratio of good to bad collisions than s-wave collisions.

[1] W. Kohn and J. M. Luttinger, New Mechanism for Superconductivity, Phys. Rev. Lett. **15**, 524 (1965).

[2] H. Kojima and H. Ishimoto, Spin polarized superfluid ^{3}He A_1, J. Phys. Soc. Jpn. **77**, 111001 (2008).

[3] M. Leduc, Spin polarized Helium-3, a playground in many domains of physics, Le Journal de Physique Colloques **51**, C6 (1990).

[4] A. P. Mackenzie, T. Scaffidi, C. W. Hicks, and Y. Maeno, Even odder after twenty-three years: The superconducting order parameter puzzle of Sr_2RuO_4, npj Quantum Mater. **2**, 40 (2017).

[5] K. Helmerson, M. Xiao, and D. Pritchard, Radiative decay of densely confined atoms, in *International Quantum Electronics Conference*, edited by A. Owyoung, C. Shank, S. Chu, and E. Ippen, Vol. 8 of OSA Technical Digest (Optical Society of America, 1990), paper QTHH4.

[6] T. Busch, J. R. Anglin, J. I. Cirac, and P. Zoller, Inhibition of spontaneous emission in fermi gases, Europhys. Lett. (EPL) **44**, 1 (1998).

[7] B. Shuve and J. H. Thywissen, Enhanced pauli blocking of light scattering in a trapped fermi gas, J. Phys. B: At., Mol. Opt. Phys. **43**, 015301 (2009).

[8] O. Morice, Y. Castin, and J. Dalibard, Refractive index of a dilute bose gas, Phys. Rev. A **51**, 3896 (1995).

[9] B. Zhu, J. Cooper, J. Ye, and A. M. Rey, Light scattering from dense cold atomic media, Phys. Rev. A **94**, 023612 (2016).

[10] A. D. Ludlow, M. M. Boyd, J. Ye, E. Peik, and P. O. Schmidt, Optical atomic clocks, Rev. Mod. Phys. **87**, 637 (2015).

[11] N. D. Lemke, J. von Stecher, J. A. Sherman, A. M. Rey, C. W. Oates, and A. D. Ludlow, p-wave Cold Collisions In An Optical Lattice Clock, Phys. Rev. Lett. **107**, 103902 (2011).

[12] B. DeMarco, J. L. Bohn, J. P. Burke, M. Holland, and D. S. Jin, Measurement Of p-Wave Threshold Law Using Evaporatively Cooled Fermionic Atoms, Phys. Rev. Lett. **82**, 4208 (1999).

[13] T. Nakasuji, J. Yoshida, and T. Mukaiyama, Experimental determination of p-wave scattering parameters in ultracold ^{6}Li atoms, Phys. Rev. A **88**, 012710 (2013).

[14] J. R. Taylor, *Scattering Theory: The Quantum Theory on Nonrelativistic Collisions* (Wiley, New York, 1972).

[15] H. Suno, B. D. Esry, and C. H. Greene, Recombination Of Three Ultracold Fermionic Atoms, Phys. Rev. Lett. **90**, 053202 (2003).

[16] J. Yoshida, T. Saito, M. Waseem, K. Hattori, and T. Mukaiyama, Scaling Law For Three-Body Collisions of Identical Fermions With p-Wave Interactions, Phys. Rev. Lett. **120**, 133401 (2018).

[17] K. Aikawa, A. Frisch, M. Mark, S. Baier, R. Grimm, and F. Ferlaino, Reaching Fermi Degeneracy Via Universal Dipolar Scattering, Phys. Rev. Lett. **112**, 010404 (2014).

[18] K. B. Davis, M. O. Mewes, M. R. Andrews, N. J. van Druten, D. S. Durfee, D. M. Kurn, and W. Ketterle, Bose-Einstein Condensation in a Gas of Sodium Atoms, Phys. Rev. Lett. **75**, 3969 (1995).

[19] Z. Hadzibabic, S. Gupta, C. A. Stan, C. H. Schunck, M. W. Zwierlein, K. Dieckmann, and W. Ketterle, Fiftyfold Improvement In The Number Of Quantum Degenerate Fermionic Atoms, Phys. Rev. Lett. **91**, 160401 (2003).

[20] B. D. Esry, C. H. Greene, and H. Suno, Threshold laws for three-body recombination, Phys. Rev. A **65**, 010705(R) (2001).

[21] X. Du, Y. Zhang, and J. E. Thomas, Inelastic Collisions of a Fermi Gas in the BEC-BCS Crossover, Phys. Rev. Lett. **102**, 250402 (2009).

[22] D. M. Stamper-Kurn, M. R. Andrews, A. P. Chikkatur, S. Inouye, H.-J. Miesner, J. Stenger, and W. Ketterle, Optical Confinement of a Bose-Einstein Condensate, Phys. Rev. Lett. **80**, 2027 (1998).

[23] A. Görlitz, T. L. Gustavson, A. E. Leanhardt, R. Löw, A. P. Chikkatur, S. Gupta, S. Inouye, D. E. Pritchard, and W. Ketterle, Sodium Bose-Einstein Condensates in the $F = 2$ State in a Large-Volume Optical Trap, Phys. Rev. Lett. **90**, 090401 (2003).

[24] J. Söding, D. Guéry-Odelin, P. Desbiolles, F. Chevy, H. Inamori, and J. Dalibard, Three-body decay of a rubidium Bose-Einstein condensate, Applied Physics B: Lasers and Optics **69**, 257 (1999).

[25] E. Nielsen and J. H. Macek, Low-Energy Recombination Of Identical Bosons By Three-Body Collisions, Phys. Rev. Lett. **83**, 1566 (1999).

[26] C. R. Monroe, E. A. Cornell, C. A. Sackett, C. J. Myatt, and C. E. Wieman, Measurement Of Cs-Cs Elastic Scattering At T=30 μk, Phys. Rev. Lett. **70**, 414 (1993).

[27] B. Zhu, G. Quéméner, A. M. Rey, and M. J. Holland, Evaporative cooling of reactive polar molecules confined in a two-dimensional geometry, Phys. Rev. A **88**, 063405 (2013).

[28] P. Zhang, P. Naidon, and M. Ueda, Scattering amplitude of ultracold atoms near the p-wave magnetic feshbach resonance, Phys. Rev. A **82**, 062712 (2010).

[29] S. Gautam and D. Angom, Scattering length for fermionic alkali atoms, Eur. Phys. J. D **56**, 173 (2010).

[30] While Ref. [13] provides a value for V_p, this value was obtained indirectly. Namely, the value was obtained by using the experimentally determined strength of a p-wave resonance which is 1.65 higher than calculated, and then multiplying a predicted value of V_p by this factor. There is no obvious reason for rescaling the theoretical value for V_p.

[31] L. Austen, Production of p-wave Feshbach molecules from an ultra-cold Fermi gas, Ph.D. thesis, University College London, 2011.

[32] C.-L. Hung, X. Zhang, N. Gemelke, and C. Chin, Accelerating evaporative cooling of atoms into Bose-Einstein condensation in optical traps, Phys. Rev. A **78**, 011604(R) (2008).

[33] W. Ketterle and M. W. Zwierlein, Making, probing and understanding ultracold Fermi gases, Riv. Nuovo Cim. **31**, 247 (2008).

[34] W. Ketterle and N. V. Druten, Evaporative Cooling of Trapped Atoms, in *Advances In Atomic, Molecular, and Optical Physics* (1996), Vol. 37.

[35] F. A. van Abeelen, B. J. Verhaar, and A. J. Moerdijk, Sympathetic cooling of ^{6}Li atoms, Phys. Rev. A **55**, 4377 (1997).

[36] S. Hensler, J. Werner, A. Griesmaier, P. O. Schmidt, A. Görlitz, T. Pfau, S. Giovanazzi, and K. Rzazewski, Dipolar relaxation in an ultra-cold gas of magnetically trapped chromium atoms, Applied Physics B: Lasers and Optics **77**, 765 (2003).

[37] M. Houbiers, H. T. C. Stoof, W. I. McAlexander, and R. G. Hulet, Elastic and inelastic collisions of ^{6}Li atoms in magnetic and optical traps, Phys. Rev. A **57**, R1497 (1998).

[38] R. Roth and H. Feldmeier, Effective s-and p-wave contact interactions in trapped degenerate Fermi gases, Phys. Rev. A **64**, 043603 (2001).

[39] Z. Idziaszek, Analytical solutions for two atoms in a harmonic trap: p-wave interactions, Phys. Rev. A **79**, 062701 (2009).